A HYBRID DENOISING APPROACH FOR SPECKLE NOISE REDUCTION IN ULTRASONIC B-MODE IMAGES

A. A. Mahmoud[1], S. EL Rabaie[1], T. E. Taha[1], O. Zahran[1], F. E. Abd El-Samie[1] and W. Al-Nauimy[2]

[1]Department of Electronics and Electrical Communications.Faculty of Electronic Engineering, Menoufia University, 32952 Menouf , Egypt.
[2]University of University of Liverpool, UK

ABSTRACT

In the literature a large number of linear and nonlinear denoising approaches for ultrasonic B-mode images. The main purpose of this paper is to test the effect of hybridization of the Log Gabor filter with the otheapproaches. The log-Gabor functions, by definition, always have no DC component, and secondly, the transfer function of the log Gabor function has an extended tail at the high frequency end. Results show that thhybridization of the Log Gabor with the Median filter gives the best output images and PSNR output values.

KEY WORDS

Image enhancement, Ultrasonic scan, Speckle noise, Denoising filters

1. INTRODUCTION

Ultrasound imaging, as a tool for medical diagnosis, is widely used in clinical practice, and in some situation sit has become a standard procedure. Although diagnostic ultrasound is considered a harmless technique and permits real-time and noninvasive anatomical scanning, B-mode images are pervaded by the speckle artifact, which results from destructive interference effects between returning echoes. This artifact introduces fine-false structures whose apparent resolution is beyond the capabilities of the imaging system, reducing image contrast and masking the real boundaries of the tissue under investigation. Its occurrence may substantially compromise the diagnostic effectiveness, introducing a great level of subjectivity in the interpretation of the images. Speckle can be defined as a destructive interference artifact and its severity depends on the relative phase between two overlapping returning echoes. Like other imaging techniques that make use of coherent sources, such as laser or radar, images from ultrasound acoustical waves are prone to speckle corruption that should be removed without affecting the important details in the image [1- 3].

Speckle differs from other types of noise in the sense that it is a deterministic artifact, meaning that two signals or images, acquired under exactly the same circumstances, will experience exactly the same speckle corruption pattern but if some or all of the circumstances differ, the speckle corruption pattern will be different. Speckle texture is usually retained in the high-intensity region [3, 4].

Log Gabor filter in the Wavelet Domain and Median filters are combined to form a hybrid denoising approach. The hybridization process is applied in two ways. Firstly, the output images from the filters are merged by Wavelet Fusion; secondly, the two filters are cascaded to the image. These two ways are explained later.

In this paper, two approaches namely, Log Gabor filter in the Wavelet Domain and Median filters are combined to form a hybrid denoising approach. The hybridization process is applied in two ways. Firstly, the output images from the filters are merged by Wavelet Fusion; secondly, the two filters are cascaded to the image. These two ways are explained below.

In this paper, a hybrid approach for ultrasonic B-mode image denoising is discussed. The paper is organized as follows, Section 2, includes details about Log Gabor filters in the Wavelet Domain. Section 3, includes details about Median filtering performance, Section 4, includes the proposed hybrid approach. Section 5, gives the simulation results followed by the conclusions and the more relevant references.

2. LOG GABOR FILTERS IN THE WAVELET DOMAIN

2.1 Discrete Wavelet Transform (DWT)

The idea of the DWT is to represent an image as a series of approximations (low pass version) and details (high pass version) at different resolutions. The image is low pass filtered to give an approximation image and high pass filtered to give detail images, which represent the information lost when going from a higher resolution to a lower resolution. Then the wavelet representation is the set of detail coefficients at all resolutions and approximation coefficients at the lowest resolution. Figure (1): (a) shows the operation of two dimensional DWT with 3-Level decomposition and (b) shows the operation of a single step decomposion -reconstruction DWT [5].

An input series is processed by two filters in parallel. h1(n) is called low pass filter (or average filter) and h2(n) is high pass filter (or difference filter). The outputs obtained are then down sampled by two so that now both the outputs are half of original length. After the first step of processing on the original series, a new series is formed with the output of the low pass filter forming the first half and the output of the high pass filter forming the second half.

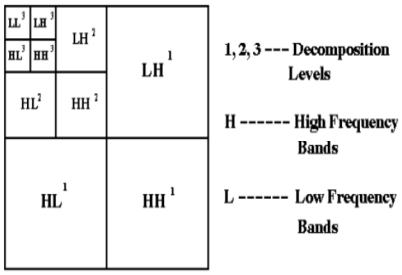

Figure (1-a) 2D-DWT with 3-Level decomposition

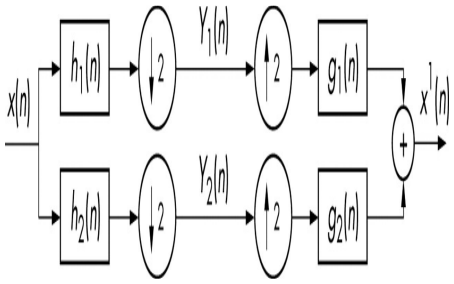

Fig. (1-b) One level of wavelet decomposition and reconstruction.

The matrix of the DWT has four subbands (LL, LH, HL, HH), the subband LL, the approximate, is the low resolution part and the subbands LH, HL, HH, the details, are the high resolution part. In the next step, only the first half of the new series that is the output of the low pass filter is processed. This kind of processing and new series formation continues till in the last step the outputs obtained from both the filters are of length one. The original length of the series needs to be a power of two so that the process of DWT can be carried untill the last step [6]. The approximate image and the detail image can be expressed as follows:-

$$Y_1(n) = \sum_{k=-\infty}^{\infty} X(k) h_1(2n-k)$$

$$Y_2(n) = \sum_{k=-\infty}^{\infty} X(k) h_2(2n-k) \quad (1)$$

where h1 is low pass filter and h2 is the high pass filter.

A Haar wavelet is the simplest wavelet type. In discrete form, Haar wavelet is related to a mathematical operation called the haar transform. The Haar transform serves as a prototype for all other wavelet transforms. The Haar decomposition has good time localization. This means that the Haar coefficients are effective for locating jump discontinuities and also for the efficient representation of images with small support. The Haar wavelet is the only known wavelet that is compactly supported, orthogonal and symmetric. It is computed by iterating difference and averaging between odd and even samples of the signal. Since we are in 2D, we need to compute the average and difference in the horizontal and then in the vertical direction [7].

Images are better coded by filters that have Gaussian transfer functions when viewed on the logarithmic frequency scale. Gabor functions have Gaussian transfer functions when viewed on the linear frequency scale. On the linear frequency scale the Log-Gabor function has a transfer function of the form:

$$G(f) = e^{\frac{-log(f/f_0)^2}{2log(\sigma/f_0)^2}} \quad (2)$$

where h1 is low pass filter and h2 is the high pass filter.

A Haar wavelet is the simplest wavelet type. In discrete form, Haar wavelet is related to a mathematical operation called the haar transform. The Haar transform serves as a prototype for all other wavelet transforms. The Haar decomposition has good time localization. This means that the Haar coefficients are effective for locating jump discontinuities and also for the efficient

representation of images with small support. The Haar wavelet is the only known wavelet that is compactly supported, orthogonal and symmetric. It is computed by iterating difference and averaging between odd and even samples of the signal. Since we are in 2D, we need to compute the average and difference in the horizontal and then in the vertical direction [7].

Images are better coded by filters that have Gaussian transfer functions when viewed on the logarithmic frequency scale. Gabor functions have Gaussian transfer functions when viewed on the linear frequency scale. On the linear frequency scale the Log-Gabor function has a transfer function of the form:

Where f0 is the filter centre frequency and σ/f0 is the ratio of the standard deviation of the Gaussian describing the log Gabor filter's transfer function in the frequency domain to the filter center frequency.

There are two important characteristics to note. Firstly, log-Gabor functions, by definition, always have no DC component, and secondly, the transfer function of the log Gabor function has an extended tail at the high frequency end [8- 10].

Where f0 is the filter centre frequency and σ/f0 is the ratio of the standard deviation of the Gaussian describing the log Gabor filter's transfer function in the frequency domain to the filter center frequency.

There are two important characteristics to note. Firstly, log-Gabor functions, by definition, always have no DC component, and secondly, the transfer function of the log Gabor function has an extended tail at the high frequency end [8- 10].

3. MEDIAN FILTERING

The Median filter is a nonlinear digital filtering technique, often used to remove noise. Such noise reduction is a typical pre-processing step to improve the results of later processing (for example, edge detection on an image). Median filtering is very widely used in digital image processing because, under certain conditions, it preserves edges while removing noise. The median of the pixel values in the window is computed, and the center pixel of the window is replaced with the computed median. Median filtering is done by, first sorting all the pixel values from the surrounding neighborhood into numerical order and then replacing the pixel being considered with the middle pixel value [11- 13].

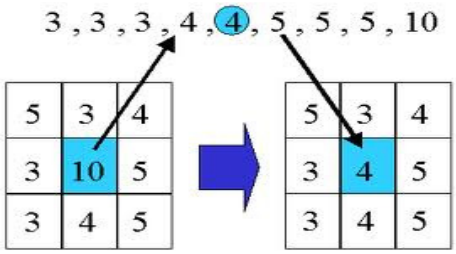

Fig. 2. Median Filtering

4. THE PROPOSED HYBRID APPROACH

In this paper, two approaches namely, Log Gabor filter in the Wavelet Domain and Median filters are combined to form a hybrid denoising approach. The hybridization process is applied in two ways. Firstly, the output images from the filters are merged by Wavelet Fusion; secondly, the two filters are cascaded to the image. These two ways are explained below.

5. WAVELET IMAGE FUSION

Image fusion is the process of combining information of interest in two or more images of a scene into a single highly informative image. Information of interest depends on the application under consideration. An image fusion system takes as an input two or more sources images and produces one fused image as an output. The key feature of hybrid architecture is the combination of advantages of pixel and region based fusion in a single image which can help the development of sophisticated algorithms enhancing the edges and structural details [14].

A schematic diagram for the fusion of two images using the DWT is depicted in Fig. 4.1. It can be defined considering the wavelet transform ω of two registered input images (image A = I1(x, y) and image B = I2(x, y)) together with the fusion rule φ. There are several wavelet fusion rules, which can be used for selecting the wavelet coefficients. The most frequently used rule is the maximum frequency rule which selects the maximum coefficients from the wavelet transformed images. Then, the inverse wavelet transform ω-1 is computed, and the fused image I(x, y) is reconstructed. Maximum frequency rule selects the coefficients with the highest absolute values. The high values indicate salient features like edges and are thus incorporated into the fused image. This rule is applied at all resolutions under consideration [15, 16].

$$I(x,y) = \omega^{-1}(\phi(\omega(I_1(x,y)), \omega(I_2(x,y)) \tag{3}$$

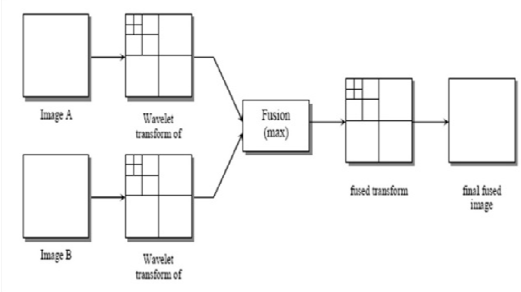

Figure 3. Wavelet fusion of two images.

- **Log Gabor Filter and Median Filter Image Fusion (Parallel Combination)**

The second way of hybridization is to apply the Log Gabor filter and the Median filter individually to the noisy image, the output images of the two filters are then merged by wavelet image fusion rule. The process is shown in figure 4.

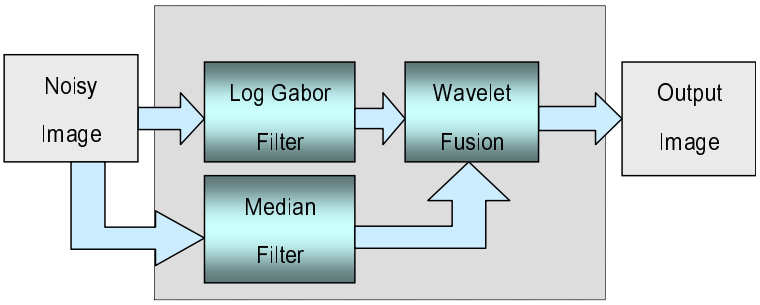

Figure 4. The Proposed Fusion Method

- **Log Gabor Filter and Median Filter Cascaded (Cascade Combination)**

The first way of hybridization is to apply the Log Gabor filter to the noisy image then apply the Median filter to the Log Gabor filter output image as shown in figure 5.

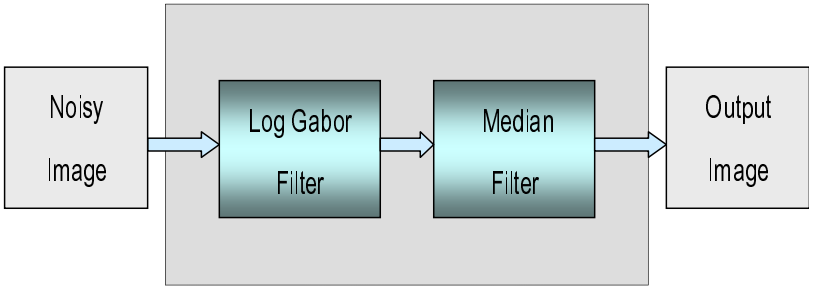

Figure 5. The Proposed Cascade Method.

6. SIMULATION RESULTS

Computer simulations were carried out using MATLAB (R2007b). The quality of the reconstructed image is specified in terms of:

- **The Peak Signal-to-Noise Ratio (PSNR) [17].**

$$PSNR = 10\ log_{10} \frac{Max\tilde{I}^2}{MSE} \tag{4}$$

Where MSE, the Mean Square Error between the estimate of the image and the original image, and is the maximum possible pixel value in the image.

$$CoC = \frac{\sum_m \sum_n [(x(m,n)-\bar{x})(y(m,n)-\bar{y})]}{\sqrt{(\sum_m \sum_n (x(m,n)-\bar{x})^2)(\sum_m \sum_n (y(m,n)-\bar{y})^2)}} \tag{5}$$

Here x (m, n) is the pixel intensity or the gray scale value at a point (m, n) in the undeformed image. y (m, n) is the gray scale value at a point (m, n) in the deformed image. and are mean values of the intensity matrices x and y, respectively.

Simulation results are conducted on six examples of ultrasonic B-mode images (Liver, Kidney, Fetus, Thyroid, Breast and Gall) [18].

Figure 6 (a) shows the ultrasonic Liver image. Speckle noise of 0.1 variance was added to the image as shown in figure 6 (b). The Median filter and the Log Gabor filter were applied to the image separately and results are shown in figures 6 (c) and 6 (d). The Wavelet fusion of the Median filter output image and the Log Gabor output image (the first hybridization case) is shown in figure 6(e). The Median filter and the Log Gabor filter were cascaded and applied to the image (the second hybridization case) and the output image is shown in figure 6 (f). Speckle noise was added to the Liver image with different variance values (0.01, 0.05, 0.1 and 0.2) and numerical results are shown in Table (1).

Figure 7 (a) shows the ultrasonic Kidney image. Speckle noise of 0.1 variance was added to the image as shown in figure 7 (b). The Median filter and the Log Gabor filter were applied to the image separately and results are shown in figures 7 (c) and 7 (d). The Wavelet fusion of the Median filter output image and the Log Gabor output image (the first hybridization case) is shown in figure 7(e). The Median filter and the Log Gabor filter were cascaded and applied to the image (the second hybridization case) and the output image is shown in figure 7 (f). Speckle noise was added to the Kidney image with different variance values (0.01, 0.05, 0.1 and 0.2). Table 2 illustrates the PSNR and CoC output values for each approach.

Figure 8 (a) shows the ultrasonic Fetus image. Speckle noise of 0.1 variance was added to the image as shown in figure 8 (b). The Median filter and the Log Gabor filter were applied to the image separately and results are shown in figures 8 (c) and 8 (d). The Wavelet fusion of the Median filter output image and the Log Gabor output image (the first hybridization case) is shown in figure 8(e). The Median filter and the Log Gabor filter were cascaded and applied to the image (the second hybridization case) and the output image is shown in figure 8 (f). Speckle noise was added to the Fetus image with different variance values (0.01, 0.05, 0.1 and 0.2). Table 3 gives the PSNR and CoC numerical results.

Figure 9 (a) shows the ultrasonic Thyroid image. Speckle noise of 0.1 variance was added to the image as shown in figure 9 (b). The Median filter and the Log Gabor filter were applied to the image separately and results are shown in figures 9 (c) and 9 (d). The Wavelet fusion of the Median filter output image and the Log Gabor output image (the first hybridization case) is shown in figure 9(e). The Median filter and the Log Gabor filter were cascaded and applied to the image (the second hybridization case) and the output image is shown in figure 9 (f). Speckle noise was added to the Thyroid image with different levels (0.01, 0.05, 0.1 and 0.2) variances and numerical PSNR and CoC output results are tabulated in Table 4.

Figure 10 (a) shows the ultrasonic Breast image. Speckle noise of 0.1 variance was added to the image as shown in figure 10 (b). The Median filter and the Log Gabor filter were applied to the image separately and results are shown in figures 4-8 (c) and 10 (d). The Wavelet fusion of the Median filter output image and the Log Gabor output image (the first hybridization case) is shown in figure 10(e). The Median filter and the Log Gabor filter were cascaded and applied to the image (the second hybridization case) and the output image is shown in figure 10 (f). Speckle noise was added to the Breast image with different variance values (0.01, 0.05, 0.1 and 0.2). Table 5 illustrates the PSNR and CoC output values for each approach.

Figure 11 (a) shows the ultrasonic Gall image. Speckle noise of 0.1 variance was added to the image as shown in figure 11 (b). The Median filter and the Log Gabor filter were applied to the image separately and results are shown in figures 11 (c) and 11 (d). The Wavelet fusion of the Median filter output image and the Log Gabor output image (the first hybridization case) is shown in figure 11(e). The Median filter and the Log Gabor filter were cascaded and applied to the image (the second hybridization case) and the output image is shown in figure 11 (f). Speckle noise was added to the Gall image with different variance values (0.01, 0.05, 0.1 and 0.2). Table

6 gives the PSNR and CoC numerical results for the filters and the proposed two hybrid approaches PSNR output values.

Table (7) illustrates the CPU times (sec) considerations for the proposed two denoising approaches.

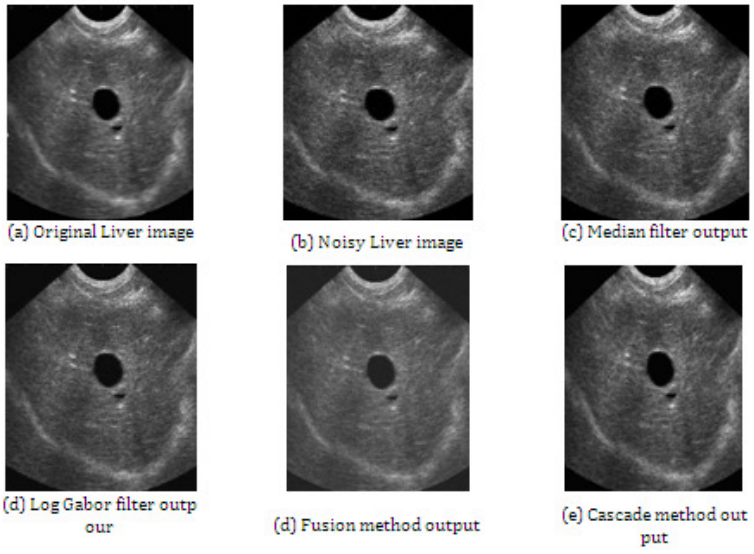

Figure 6. Output Liver images of the mentioned filters and the proposed approaches.

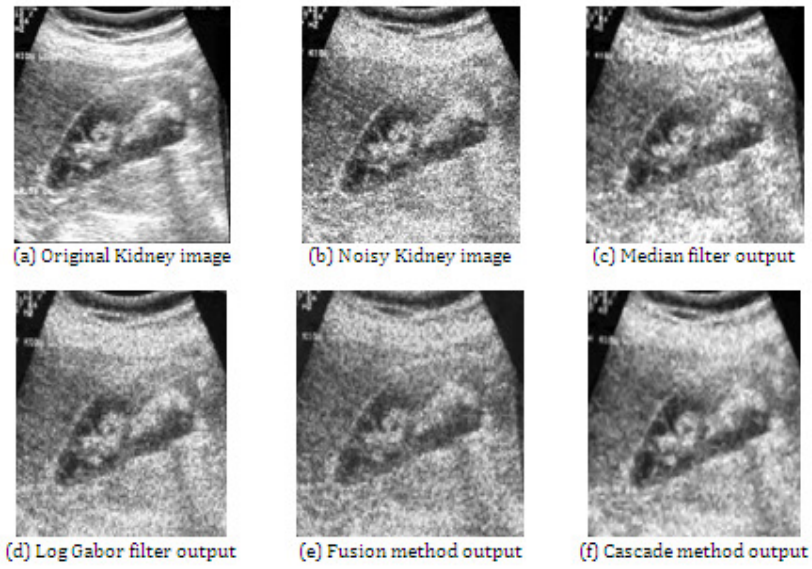

Figure 7. Output Kidney images of the mentioned approaches and the proposed approaches.

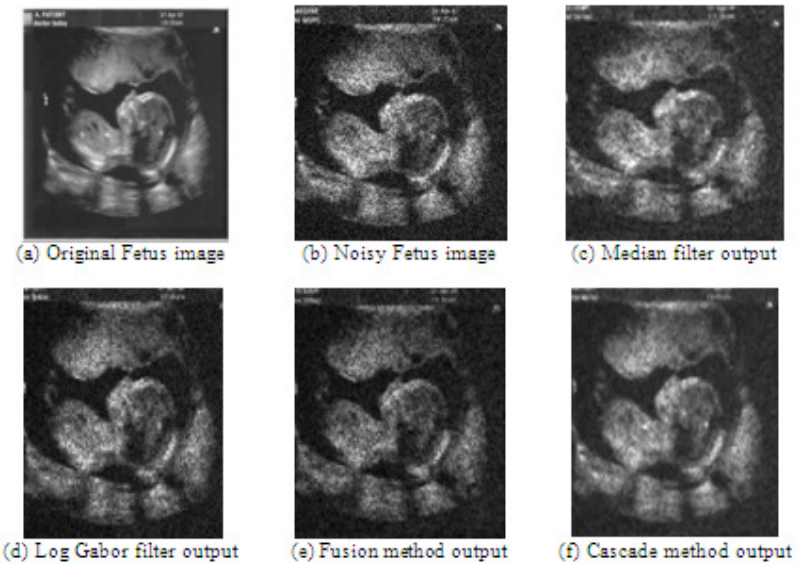

Figure 8. Output Fetus images of the mentioned filters and the proposed approaches.

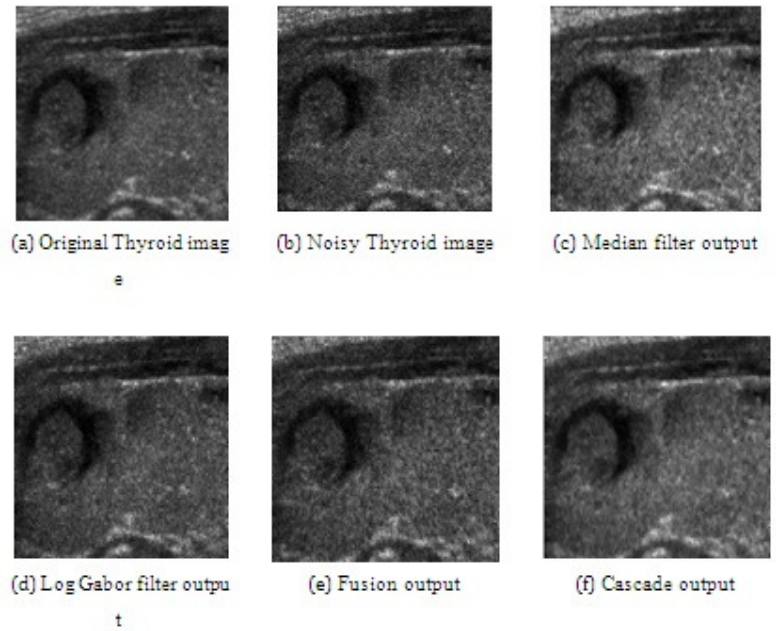

Figure 9. Output Thyroid images of the mentioned filters and the proposed approaches.

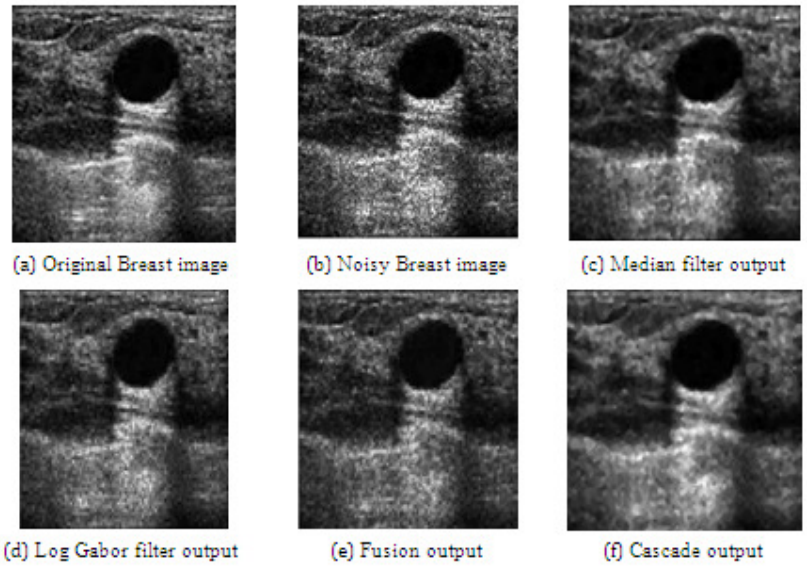

Figure 10. Output Breast images of the mentioned filters and the proposed approaches.

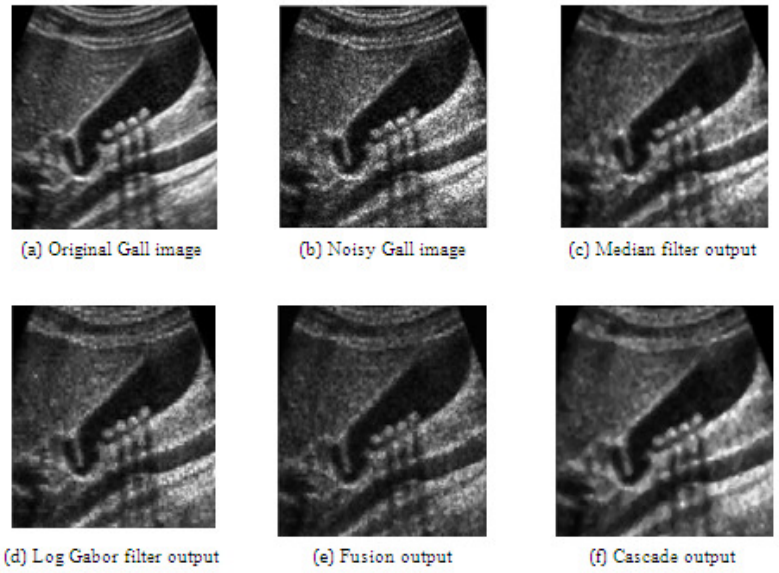

Figure 11. Output Gall images of the mentioned filters and the proposed approaches.

Table (1) PSNR and CoC output values of the denoising approaches applied to the Liver image with speckle noise variance of (0.01: 0.2).

The first example (Liver image)				
Approaches	*Noise variance*			
	0.01	***0.05***	***0.1***	*0.2*
PSNR $_{Noisy}$	31.51	25.97	23.92	22.04
PSNR $_{Fusion}$	33.01	29.44	27.27	26.22
PSNR $_{Cascade}$	**30.56**	**29.82**	**29.28**	**28.00**
CoC $_{Noisy}$	0.7550	0.8523	0.9172	0.9817
CoC $_{fusion}$	0.8485	0. 9108	0.9484	0.9833
CoC $_{Cascade}$	**0.9316**	**0.9564**	**0.9687**	**0.9798**

Table (2) PSNR and CoC output values of the denoising approaches applied to the Kidney image with speckle noise variance of (0.01: 0.2).

The second example (Kidney image)				
Approaches	*Noise variance*			
	0.01	***0.05***	***0.1***	***0.2***
PSNR $_{Noisy}$	23.03	20.52	18.42	16.60
PSNR $_{Fusion}$	26.01	23.27	21.63	21.01
PSNR $_{Cascade}$	**24.18**	**23.72**	**22.93**	**21.99**
CoC $_{Noisy}$	0.9792	0.9076	0.8393	0.7303
CoC $_{fusion}$	0.9764	0.9445	0.9077	0.8499
CoC $_{Cascade}$	**0.9683**	**0.9562**	**0.9437**	**0.9169**

Table (3) PSNR and CoC output values of the denoising approaches applied to the Fetus image with speckle noise variance of (0.01: 0.2).

The third example (Fetus image)				
Approaches	*Noise variance*			
	0.01	***0.05***	***0.1***	***0.2***
PSNR $_{Noisy}$	29.54	23.98	21.94	20.16
PSNR $_{Fusion}$	27.47	26.40	25.05	23.86
PSNR $_{Cascade}$	**31.50**	**28.93**	**27.29**	**25.52**
CoC $_{Noisy}$	0.9813	0.9154	0.8496	0.7565
CoC $_{fusion}$	0.9629	0.9328	0.8963	0.8318
CoC $_{Cascade}$	**0.9669**	**0.9547**	**0.9393**	**0.9000**

Table (4) PSNR and CoC output values of the denoising approaches applied to the Thyroid image with speckle noise variance of (0.01: 0.2).

The fourth example (Thyroid image)				
Approaches	*Noise variance*			
	0.01	***0.05***	***0.1***	***0.2***
$PSNR_{Noisy}$	29.19	24.14	21.73	20.09
$PSNR_{Fusion}$	29.94	26.70	24.83	22.32
$PSNR_{Cascade}$	**29.70**	**27.83**	**26.59**	**24.82**
CoC_{Noisy}	0.9655	0.8591	0.7609	0.6366
CoC_{fusion}	0.9654	0.9188	0.8704	0.7885
$CoC_{Cascade}$	**0.9602**	**0.9416**	**0.9190**	**0.8767**

Table (5) PSNR and CoC output values of the denoising approaches applied to the Breast image with speckle noise variance of (0.01: 0.2).

The fifth example (Breast image)				
Approaches	*Noise variance*			
	0.01	***0.05***	***0.1***	***0.2***
$PSNR_{Noisy}$	30.28	24.99	22.38	20.83
$PSNR_{Fusion}$	26.34	25.04	24.63	23.81
$PSNR_{Cascade}$	**25.38**	**24.97**	**24.79**	**24.41**
CoC_{Noisy}	0.9835	0.9243	0.8645	0.7738
CoC_{fusion}	0.9635	0.9369	0.9106	0.8570
$CoC_{Cascade}$	**0.9494**	**0.9389**	**0.9268**	**0.9028**

Table (6) PSNR and CoC output values of the denoising approaches applied to the Gall image with speckle noise variance of (0.01: 0.2).

The sixth example (Gall image)				
Approaches	*Noise variance*			
	0.01	***0.05***	***0.1***	***0.2***
$PSNR_{Noisy}$	30.40	24.65	22.54	20.72
$PSNR_{Fusion}$	29.33	26.54	25.22	23.22
$PSNR_{Cascade}$	**27.34**	**26.99**	**26.21**	**25.42**
CoC_{Noisy}	0.9849	0.9297	0.8755	0.7875
CoC_{fusion}	0.9812	0.9486	0.9153	0.8515
$CoC_{Cascade}$	**0.9762**	**0.9642**	**0.9495**	**0.9292**

Table (7) CPU time output values of the denoising approaches applied to the six examples.

The six examples						
	Liver	Kidney	Fetus	Thyroid	Breast	Gall
CPU_{Fusion}	6.71	1.29	1.20	1.28	0.64	0.58
$CPU_{Cascade}$	**5.83**	**1.02**	**0.90**	**1.04**	**0.47**	**0.37**

For the Liver image, the two cases are tested. The PSNR decreases for the lower noise levels because the proposed approaches have no effect when the PSNR values are high. The cascade case improves the PSNR especially at high noise levels by nearly 1.78 db and the output images quality are better as compared to the fusion case.

The output PSNR values for the Kidney image of the two cases are very close to each other. The cascade case improves the PSNR output values at 0.2 speckle noise variance by nearly 0.98 db and its output images are better.

For the third and the fourth examples, the Fetus and Thyroid images, not only the PSNR output values for the fusion case decreases heavily but also the output images quality. On the other hand, the cascade case improves the PSNR output values at 0.2 speckle noise variance by nearly 1.66 db for the third example and 2.5 db for the fourth example also the output images quality increased for the cascade case.

The output PSNR values for the fifth example, the Breast image, the two cases performs very close to each other. The PSNR output values decreases for the low speckle noise levels, but the cascade case output images and PSNR values are improved for high noise variances. The cascade case improves the PSNR at 0.2 speckle noise variance by nearly 1.4 db.

For the last example, the Gall image, the PSNR decreases for the lower noise levels and the output images quality are not very good for the fusion case. The cascade case improves the PSNR output values at 0.2 speckle noise variance by nearly 2.2 db and the output images quality are better than the fusion case. The cascade case improves the CoC output values for the six examples over those for the fusion case at 0.2 speckle noise variance by 0.0831, 0.067, 0.0682, 0.0882, 0.0458, and .0.0777 respectively.

Results demonstrate that the second approach (the cascade combination approach) gives the best results when applied to the ultrasonic speckled images.

7. CONCLUSIONS

This paper presents two cases of hybridization, fusion (parallel) and (cascade).Th. Results show that the Log-Gabor filter gives the best denoising performance when combined with the median filter in parallel and cascade combination. The two cases of hybridization are tested on the ultrasonic images and the second case (cascade case) has successful denoising performance especially at high speckle noise levels.

REFERENCES

[1] R. G. Dantas and E.T. Costa, "Ultrasound speckle reduction using modified gabor filters", IEEE Trans., Ultrason., Ferroelectr., Freq. Control, vol 54, pp. 530 – 538, 2007.

[2] O. V. Michailovich and A. Tannenbaum, "Despeckling of medical ultrasound images", IEEE Trans. Ultrason., Ferroelectr., Freq. Control, vol 53(1), pp. 64-78, 2006.

[3] J. R. Sanchez and M. L. Oelze, "An ultrasonic imaging speckle suppression and contrast enhancement technique by means of frequency compounding and coded excitation", IEEE Trans. Ultrason. Ferroelectr., Freq. Control, vol. 56, no. 7, 2009.

[4] X. Zong, A.F. Laine, and E. A. Geiser, "Speckle reduction and contrast enhancement of echocardiograms via multiscale nonlinear processing", IEEE Trans. Medical Imaging, vol.17, pp.532-540, Aug. 1998.

[5] L. Kaur, S. Gupta, and R. C. Chauhan, "Image denoising using wavelet thresholding", Third Conference on Computer Vision, Graphics and Image Processing, India Dec 16-18, 2002.

[6] S. Kother Mohideen, S. Arumuga Perumal and M. Mohamed Sathik, "Image denoising using discrete wavelet transform", International Journal of Computer Science and Network Security, vol. 8, no. 1, Jan., 2008.

[7] N. Jacob and A. Martin. "Image denoising in the wavelet domain using wiener filtering", University of Wisconsin, Madison, Wisconsin, USA, 2004.

[8] R. Zewail, A. Seil, N. Hamdy and M. Saeb," Iris identification based on log-gabor filtering", Proceedings of the IEEE Midwest Symposium on Circuits, Systems & Computers, vol. 1, pp 333-336, Dec. 2003.

[9] A. Karargyris, S. Antani and G. Thoma, "Segmenting anatomy in chest x-rays for tuberculosis screening", Engineering in Medicine and Biology Society, EMBC, Annual International Conference of the IEEE: 7779-82, Aug. 2011.

[10] P. Kovesi, "Phase preserving denoising of images", Proc. DICTA 99 (Perth, Australia), pp. 212- 217, 1999.

[11] S. Dangeti, "De-noising techniques a comparison", Andhra University, Vishakapatnam, May, 2003

[12] S. Perreault, P. Hébert, "Median filtering in constant time", IEEE Trans. on Image Processing 16(9): 2389-2394, 2007.

[13] Y. Mi, X. Li and G. F. Margrave, "Application of median filtering in Kirchhoff migration of noisy data", CREWES Research Report, 49, 11, 1999.

[14] T. Zaveri and M. Zaveri, "A novel two step region based multifocus image fusion method", International Journal of Computer and Electrical Engineering, Vol. 2, No. 1, 1793-8163. pp. 86-91[9], February, 2010.

[15] A. ben Hamza, Yun He, Hamid Krim, and Aln Willsky, "A multiscale approach to pixel-level image fusion," Integrated Computer-Aided Engineering, IOS Press, vol. 12, pp. 135- 146, 2005.

[16] F. E. Ali, I. M. El-Dokany, A. A. Saad, and F. E. Abd El-Samie., "Curvelet fusion of mr and ct images," Progress In Electromagnetics Research C, vol. 3, 215-224, 2008.

[17] Q .Huynh-Thu,M. Ghanbari ,"Scope of validity of PSNR in image/video quality assessment", Electronics Letters, vol. 44,No.13,pp.800–801, 2008.

[18]http://www.google.com.eg/search ultrasonic image, [Date of access, Dec. 2011].